Nano Research 2018, 11(7): 3548–3554
https://doi.org/10.1007/s12274-017-1920-9
Research Article
ISSN 1998-0124
CN 11-5974/O4

A sustainable aqueous Zn-I_2 battery

Chong Bai[1,§], Fengshi Cai[2,§], Lingchang Wang[2], Shengqi Guo[2], Xizheng Liu[2] (✉), and Zhihao Yuan[1,2] (✉)

[1] *School of Materials Science and Engineering, Tianjin University, Tianjin 300072, China*
[2] *School of Materials Science and Engineering, Tianjin Key Lab for Photoelectric Materials & Devices, Tianjin University of Technology, Tianjin 300384, China*
[§] *Chong Bai and Fengshi Cai contributed equally to this work.*

Received: 20 September 2017
Revised: 1 November 2017
Accepted: 11 November 2017

KEYWORDS
aqueous battery,
nanoporous carbon,
iodine,
zinc,
cycle life

ABSTRACT

Rechargeable metal-iodine batteries are an emerging attractive electrochemical energy storage technology that combines metallic anodes with halogen cathodes. Such batteries using aqueous electrolytes represent a viable solution for the safety and cost issues associated with organic electrolytes. A hybrid-electrolyte battery architecture has been adopted in a lithium-iodine battery using a solid ceramic membrane that protects the metallic anode from contacting the aqueous electrolyte. Here we demonstrate an eco-friendly, low-cost zinc-iodine battery with an aqueous electrolyte, wherein active I_2 is confined in a nanoporous carbon cloth substrate. The electrochemical reaction is confined in the nanopores as a single conversion reaction, thus avoiding the production of I_3^- intermediates. The cathode architecture fully utilizes the active I_2, showing a capacity of 255 mAh·g^{-1} and low capacity cycling fading. The battery provides an energy density of ~ 151 Wh·kg^{-1} and exhibits an ultrastable cycle life of more than 1,500 cycles.

1 Introduction

The pursuit of reliable, low-cost, and eco-friendly electrochemical energy storage devices is mainly motivated by energy crises and looming environmental concerns [1, 2]. Among various energy storage paradigms [3, 4], rechargeable metal-iodine batteries (MIBs) are one of the most attractive candidates due to their high energy density, low-cost, and abundant iodine resources [5, 6]. A rechargeable Li-I_2 battery was initially proposed in the 1970s, and it had a cycle life of more than 100 cycles. Related works have been presented in the following decades [7–9]. Very recently, interest in various MIBs (Na-I_2 [10], Mg-I_2 [11], Al-I_2 [12]) has increased because of advanced analysis techniques and thriving application of nanotechnology for electrodes fabrication. However, the reported batteries are constructed using flammable and toxic organic electrolytes, thus raising safety concerns. Hybrid-electrolyte Li-I_2 batteries both in static and flow models were systematically investigated by Zhao et al. [13, 14]. In these batteries, a Li-only conductive

Address correspondence to Xizheng Liu, xzliu@tjut.edu.cn; Zhihao Yuan, zhyuan@tjut.edu.cn

ceramic membrane (LATP) was employed to separate the metallic Li anode and the aqueous cathode. The batteries demonstrated a high voltage (~ 3.5 V), high Coulombic efficiency (~ 100%), and notable energy density (~ 0.33 kWh·kg^{-1}). Further, the use of a low-cost, eco-friendly aqueous catholyte favored large-scale storage applications. However, the flammable organic anolyte and high-cost solid-state LATP membrane caused safety concerns. Therefore, MIBs using only aqueous electrolytes are urgently required.

Among aqueous MIBs, the Zn-I_2 couple, which is based on the reversible conversion reaction Zn + I_2 ↔ ZnI_2, is a promising candidate. Metallic zinc is a high energy density anode and is stable in water. Compared to rechargeable Li-ion batteries, which use organic electrolytes, Zn-air batteries, which have a limited cycle life, the Zn-I_2 couple demonstrates improved safety because of the use of a mild aqueous electrolyte and the fast redox reaction. These features increase the possibility of high cycling performance. A Zn-I_2 prototype battery was first reported in the 1980s, but its development was plagued by a series of problems such as lack of appropriate iodine carriers, severe self-discharge, and Zn dendritic growth during cycling [15]. Recently, the battery performance has been improved by conversion of the aqueous I_3^-/I^- couple [16, 17]. However, storing an electroactive species in electrolytes limits the atom utilization efficiency of the iodine species and the battery energy density. To extend the scope of battery application and investigate new electrochemical reactions, the active iodine species requires to be robustly confined in the solid cathode, where the corresponding electrochemical reaction also occurs.

Herein, we demonstrate an aqueous rechargeable Zn-I_2 battery (ZIB). There are two favorable features of the proposed architecture. 1) Iodine is strategically infused into a conductive nanoporous activated carbon cloth (ACC) by sublimation of I_2, which drastically enhances battery performance; 2) a non-flammable and environmentally benign aqueous electrolyte instead of a toxic organic electrolyte is employed. This facilitates the preparation of safe and eco-friendly batteries. The achieved ZIBs exhibit a high specific capacity (255 mAh·g^{-1} at 0.5 C) and long-term cyclability (> 1,500 cycles) at ≥ 99% Coulombic efficiency at a high current rate (5 C). Moreover, the batteries demonstrate superior electrochemical stability with a high capacity retention of 87% over a 30-day rest period.

2 Experimental

2.1 Preparation of ACC/I_2 cathodes

Briefly, a commercial nanoporous ACC was treated with dilute HCl solution. Certain amount of iodine (Sinopharm Chemical Reagents Co., Ltd., 99.9%) was then mixed with the ACC in a stainless-steel reactor. The reactor was heated to 80 ℃ for 10 min. The iodine content in the ACC was determined by subtracting the mass of the ACC from that of the obtained ACC/I_2 composite.

2.2 Material characterization

The morphology and elemental mapping of the materials were studied using a ZEISS MERLIN microscope at 5 kV. Surface area and pore size distribution were determined using a surface area and pore size analyzer (Micromeritics ASAP2020) at 77 K. X-ray photoelectron spectroscopy (XPS) analysis was performed on a Thermo ESCALAB 250 instrument configured with monochromatic Al Kα radiation (1,486.6 eV). X-ray diffraction (XRD) measurements were performed using a Rigaku Miniflex II diffractometer with Cu Kα radiation (λ = 1.5406 Å). Thermogravimetric analysis was conducted using a NETZSCH TG-DSC analyzer. The heating rate was 5 ℃·min^{-1} from room temperature to 500 ℃ under Ar atmosphere. Raman measurements were performed on a HORIBA/LabRAM HR Evolution microscope using a 532-nm diode-pumped solid-state laser. An aqueous solution of 0.01 M I_2 and 0.1 M KI was characterized as reference for the I_3^- species. The positive electrodes at different voltage stages were exfoliated from batteries and detected instantly without washing. For post-mortem scanning electron microscopy (SEM) studies, cells were disassembled in air and the electrodes were collected and rinsed thoroughly with distilled water.

2.3 Electrochemistry

Aqueous electrolytes, namely, zinc sulfate, zinc nitrate,

and zinc acetate, were prepared as 1 M solutions. Linear sweeping voltammetry of the electrolytes was performed in three-electrode vial cells with a stainless-steel mesh as the working electrode, zinc as the counter electrode, and saturated calomel electrode as the reference electrode. Cyclic voltammetry of the electrolytes was carried out using zinc as the reference electrode. The ACC/I_2 composite was used as the cathode directly and punched into 2 cm^2 electrode coins. The iodine loading was ~ 4.5 $mg \cdot cm^{-2}$. Zinc foil (Sinopharm Chemical Reagents Co., Ltd, 99.5%) of thickness 0.2 mm was cut into a disc of 16 mm diameter and polished with sandpaper before use. The ZIBs were assembled in air using ~ 100 μL of 1 M $ZnSO_4$ aqueous electrolyte and filter paper as separators. The cycling characteristics of the cells were assessed under galvanostatic conditions with a Land battery measurement system (Wuhan, China). The current density was based on the weight of iodine (1 C = 211 $mA \cdot g^{-1}$). Cyclic voltammetry was performed on a ZAHNER Thales electrochemistry workstation.

3 Results and discussion

The ZIB was constructed by an ACC/I_2 cathode, a Zn anode, and a mild aqueous zinc sulfate electrolyte, as displayed in Fig. 1(a). The fibers of the ACC are nanoporous and get impregnated with iodine due to iodine's low sublimation temperature. Iodine species transforms between iodine and iodide in nanopores of the ACC during cycling, while zinc ions undergo reversible stripping/deposition on anodes correspondingly. The morphology of the prepared ACC/I_2 cathode was examined by SEM, as shown in Fig. 1(b). There is no residual I_2 on the ACC surface, and the elemental mapping images demonstrate that elemental iodine is homogeneously distributed within the carbon fibers (Fig. 1(c)). The specific surface area reduced from 1,040 to 800 $m^2 \cdot g^{-1}$ after I_2 impregnation (Fig. 1(d) and Fig. S1 in the Electronic Supplementary Material (ESM)), which demonstrates that I_2 is trapped inside the nanopores. The XRD patterns of the ACC/I_2 composite display no crystalline iodine peaks as I_2 is sequestered (Fig. S2 in the ESM). In addition, the X-ray photoelectron spectroscopy analysis depict iodine to be mostly physically adsorbed by carbon (Fig. S3 in the ESM) [18]. The physical confinement by the porous structure and good affinity of carbon to iodine significantly improve the thermostability of I_2, which was verified by thermogravimetric analysis curves (Fig. 1(e)). No mass loss of I_2 is observed below 180 °C after being strategically infused into the ACC.

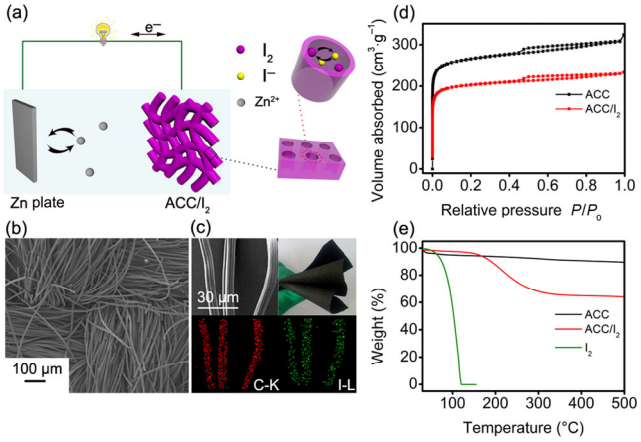

Figure 1 (a) Schematic of ZIB architecture using I_2-loaded carbon cloth as cathode and detailed cathode structure. (b) SEM image of ACC/I_2 composite. (c) Photograph and elemental mapping profiles of elemental C and I of ACC/I_2 composite. (d) N_2-adsorption-desorption isotherm profiles of ACC/I_2 composite. (e) Thermogravimetric analysis curves of ACC/I_2 composite.

We first screened the aqueous electrolytes, namely, zinc sulfate, zinc acetate, and zinc nitrate (Fig. S4 in the ESM). The potentiodynamic behaviors of the Zn electrodes were compared, and the voltammetry in $ZnSO_4$ showed reversible electrochemical deposition/stripping of Zn, while different processes were observed in $Zn(Ac)_2$ and $Zn(NO_3)_2$ solutions because of the low activity of acetate ions and NO_3^-. Moreover, the undesirable reaction of O_2 evolution was obviously suppressed in 1 M $ZnSO_4$, and a wide working potential window of ~ 2.4 V was observed. Accordingly, 1 M $ZnSO_4$ aqueous solution was adopted as the electrolyte.

Typical galvanostatic discharge/charge curves at 0.5 C are shown in Fig. 2(a). A very high capacity of 255 $mAh \cdot g^{-1}$ is obtained, which is higher than the theoretical capacity of I_2 and that of previously reported ZIBs [15]. This is attributed to the capacitance behavior of the ACC (Fig. S5 in the ESM). Different from two pairs of plateaus observed for organic MIBs, only one pair of pronounced flat plateaus at ~ 1.2 V is observed, which suggests a different electrochemical

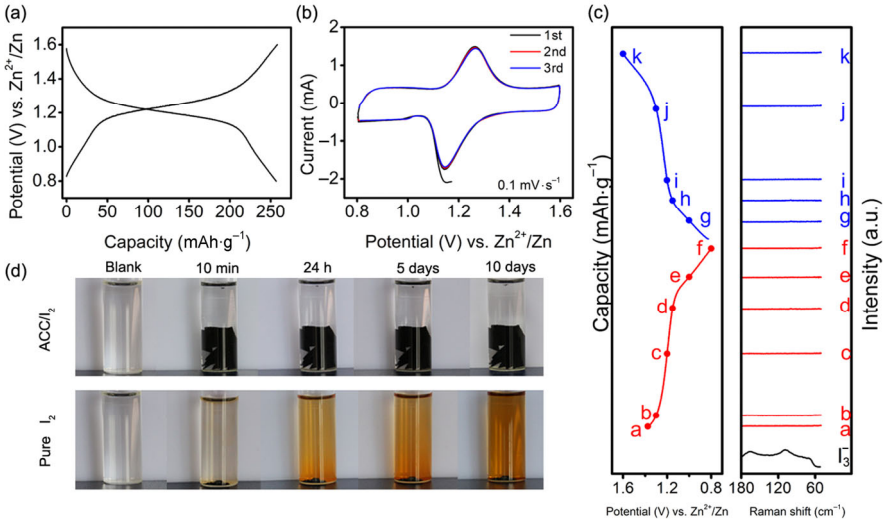

Figure 2 (a) Typical galvanostatic discharge/charge profiles at 0.5 C rate. (b) Cyclic voltammograms in the initial three cycles. (c) Raman spectra of ACC/I_2 cathode at different voltage states in cycling. The black line is the reference spectrum of I_3^-. (d) Dissolution behaviors of ACC/I_2 cathode. ACC/I_2 composite and equal weight of iodine (~ 60 mg) were immersed into electrolyte solution.

reaction mechanism.

To understand the reaction mechanism, cyclic voltammograms were obtained (Fig. 2(b)). The initial three cycles almost overlap, proving that the electrochemical reaction is highly reversible. A wide horizontal region with capacitive characteristics is further related to capacitance behavior. The peak currents versus square root of scan rates is linear, demonstrating diffusion-controlled behavior (Fig. S6 in the ESM).

One pair of redox peaks was obtained, as opposed to the case of previously reported non-aqueous MIBs. In typical two-step MIBs, the cathode reaction can be described as $I_2 \leftrightarrow I_3^- \leftrightarrow I^-$. This reaction pathway decreases I_2 utilization efficiency and limits the battery energy density. Our presented results, just like all solid-state Li-I_2 batteries [19], involve a single conversion process of iodine to iodide ions without polyiodide intermediates. To confirm this hypothesis, the ZIB is operated at −2 ˚C. The kinetics of the discharge are lowered to deconvolute any multi-step plateaus that would otherwise be smeared [20]. The discharge capacity declines due to low temperature, and a single two-phase region is demonstrated obviously at ~ 1.2 V (Fig. S7 in the ESM). Additionally, no characteristic signals of polyiodide, which are usually located around 120 and 110 cm^{-1} [21], are detected in the Raman spectra of the ACC/I_2 electrode at different states of charge (Fig. 2(c)). The absence of polyiodide significantly improves cycling stability, as the diffusion of highly soluble intermediates in the electrolyte undoubtedly deteriorates the cycle performance [22]. Additionally, the absence of polyiodide circumvents the employment of special electrolyte additives or ultra-high concentration electrolytes, which are adopted to alleviate the disadvantages of polyiodide intermediate [11, 23]. The dissolution behavior of the ACC/I_2 cathode in the electrolyte was also studied. The color of the electrolyte did not change even after 10 days (Fig. 2(d)), proving that the dissolution of I_2 is highly impeded by incorporation of I_2 within the nanoporous ACC.

Figure 3(a) displays long cycling stability of galvanostatic discharge/charge. Only a slight performance fading in the specific capacity and voltage profiles is observed. The battery performance is further reflected in the rate performance (Fig. 3(b)). Even at a high rate of 5 C, the batteries deliver a high capacity and stable performance, and when the current is decreased, the capacity is almost restored. Further long-term measurements show a high capacity retention (Fig. 3(c)) as the capacity decreases from ~ 240 to 220 $mAh \cdot g^{-1}$ after 500 cycles at 1 C. Even at 5 C (Fig. 3(d)), an impressive ~ 90% of the highest achievable capacity (160 $mAh \cdot g^{-1}$) is available after 1,500 cycles. The Coulombic efficiency (≥ 99% for the cycling duration and all rates) points to quantitative utilization of

the electrical charge. Studies on cycling performance suggest that ZIBs have much higher reversibility and durability than reported non-aqueous MIBs [10–12]. The morphology and elemental mapping of the ACC/I_2 cathode after long-term cycling were also studied. The surface is smooth without any obvious phase change, and the elemental iodine is homogeneously distributed within the carbon fibers even after 300 cycles, proving iodine's robust confinement in the nanoporous ACC (Fig. 3(e) and Figs. S8 and S9 in the ESM). The superior electrochemical performance should also ascribe to stability of the Zn anode in the aqueous $ZnSO_4$ electrolyte. In the near-neutral electrolyte, the zincate ions $[Zn(OH)_4]^{2-}$, which initiate dendritic growth, do not appear. No dendritic growth on the Zn surface is further confirmed in the post-mortem analysis of the cells (Fig. S10 in the ESM).

Severe self-discharge is a notorious obstacle in the practical application of MIBs [24]. Therefore, capacity profiles of ZIBs after a long duration of rest were studied (Figs. 4(a) and 4(b)). The battery was galvanostatically cycled and then rested at open circuit.

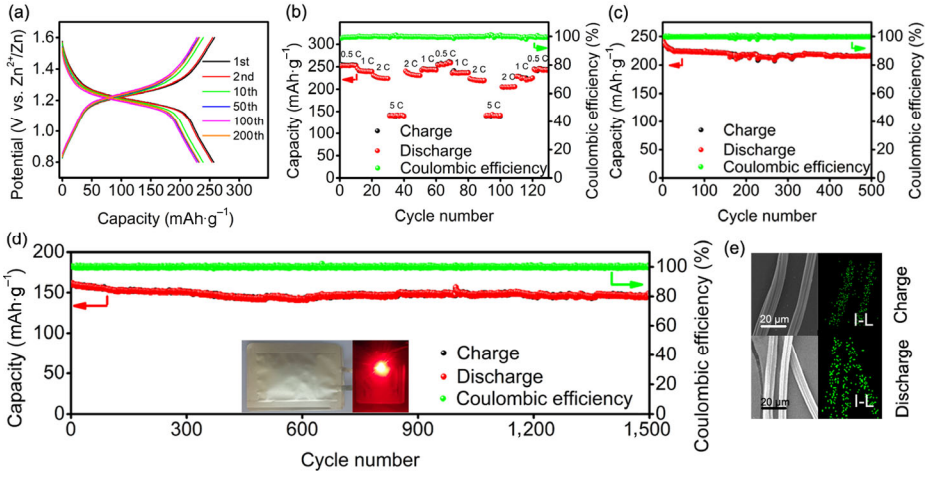

Figure 3 (a) Comparative cycling performance at 0.5 C for 200 cycles. (b) Rate capability at varying C rates. (c) Long-term cycling performance at 1 C for 500 cycles. (d) Extended cycling performance at 5 C with > 90% capacity retention (with respect to the highest capacity of 160 mAh·g^{-1}) maintained after 1,500 cycles. The insets are images of lab-scale ZIB. (e) The mapping profiles of elemental iodine of ACC/I_2 cathode after 300 cycles.

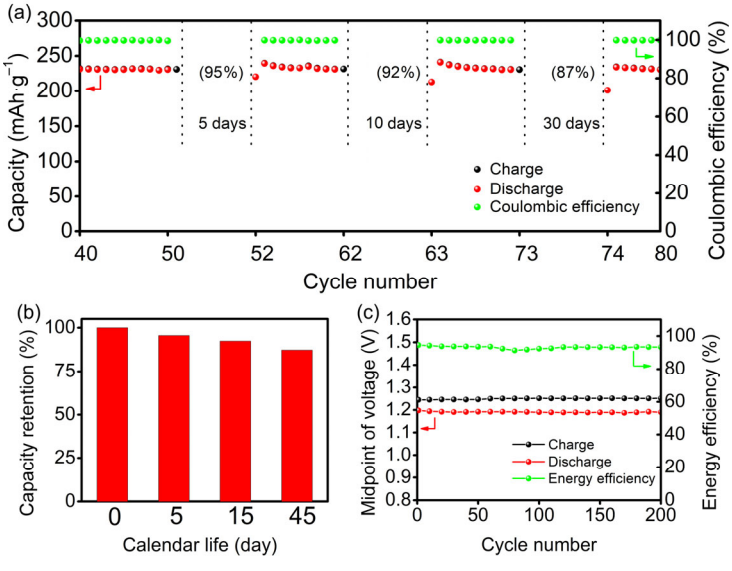

Figure 4 (a) Galvanostatic discharge and charge capacity profiles and corresponding Coulombic efficiency of ZIBs. (b) Capacity retention of ZIBs after resting at open circuit. (c) Overpotential and energy efficiency profiles of ZIBs.

Even after 30 days, the battery still showed 87% capacity, indicating that self-discharge is highly mitigated. The performance is superior to that of conventional aqueous batteries [25]. Additionally, the Coulombic efficiency was still around 100% after resting. These phenomena are associated with the good confinement of I_2 to the ACC. Iodine was strongly immobilized in the pores of the ACC, which effectively restrained iodine diffusion to the anode. Furthermore, the ZIBs displayed a high energy efficiency of > 90% with a minor voltage gap of ~ 50 mV between charge and discharge at the midpoint of the voltage profiles during long-term cycling (Fig. 4(c)). This is the best result among those obtained for previously reported organic MIBs [10–12] and can be ascribed to the following: 1) the intentional impregnation of electronic insulating I_2 in the nanopores of conductive ACC fibers improving conductivity of the composite electrode and 2) the ionic conductivities of aqueous electrolytes (up to 1 $S{\cdot}cm^{-1}$) being much higher than those of non-aqueous ones (~ 1–10 $mS{\cdot}cm^{-1}$), which facilitates electron transportation.

The combination of superior reversible ACC/I_2 cathodes, dendrite-free Zn anodes, and energetic conversion reaction entails high-performance ZIBs. A lab-scale cell was also assembled to estimate the practical utilization potential of the as-prepared ZIBs. The cell delivered a specific energy of 151 $Wh{\cdot}kg^{-1}$ using iodine and zinc metal, which is much higher than that of aqueous lithium-ion batteries [26–28]. After the initial 50 cycles, the capacity changed negligibly (Fig. S11 in the ESM).

4 Conclusions

In conclusion, high-performance rechargeable aqueous ZIBs based on nanoporous activated carbon cloth/iodine cathodes are demonstrated here. Iodine is strongly confined by the porous carbon fibers and undergoes a conversion reaction without the formation of polyiodide intermediates. A high reversible energy density of 151 $Wh{\cdot}kg^{-1}$, a capacity retention of more than 90% after 1,500 cycles, and a high capacity retention of 87% after extended rest time are observed. The combination of the superior electrochemical performance, an aqueous electrolyte, and ease of overall battery assembly helps in meeting the requirements of high-performance, eco-friendly, and safe energy storage applications.

Acknowledgements

This work was financially supported by the National Natural Science Foundation of China (Nos. 21171128 and 21603162), Tianjin Sci. & Tech. Program (No. 17JCYBJC21500), and the Fundamental Research Funds of Tianjin University of Technology.

Electronic Supplementary Material: Supplementary material (the pore size distribution, XRD and XPS patterns of ACC/I_2 composite, CV profiles of electrolytes, capacitance behaviors of ACC, CV profiles of ACC/I_2 composite, discharge profiles of cell at low temperature, XRD patterns and SEM images of ACC/I_2 cathodes after 300 cycles, SEM images of Zn anodes, cycling performance of lab-scale cell) is available in the online version of this article at https://doi.org/10.1007/s12274-017-1920-9.

References

[1] Dunn, B.; Kamath, H.; Tarascon, J.-M. Electrical energy storage for the grid: A battery of choices. *Science* **2011**, *334*, 928–935.

[2] Sun, Y. M.; Liu, N.; Cui, Y. Promises and challenges of nanomaterials for lithium-based rechargeable batteries. *Nature Energy* **2016**, *1*, 16071.

[3] Feng, N. N.; He, P.; Zhou, H. S. Critical challenges in rechargeable aprotic Li–O_2 batteries. *Adv. Energy Mater.* **2016**, *6*, 1502303.

[4] Hu, Z.; Liu, Q. N.; Chou, S.-L.; Dou, S.-X. Advances and challenges in metal sulfides/selenides for next-generation rechargeable sodium-ion batteries. *Adv. Mater.* **2017**. DOI: 10.1002/adma.201700606.

[5] Park, M.; Ryu, J.; Wang, W.; Cho, J. Material design and engineering of next-generation flow-battery technologies. *Nat. Rev. Mater.* **2016**, *2*, 16080.

[6] Zhao, Y.; Ding, Y.; Li, Y. T.; Peng, L. L.; Byon, H. R.; Goodenough, J. B.; Yu, G. H. A chemistry and material perspective on lithium redox flow batteries towards high-density electrical energy storage. *Chem. Soc. Rev.* **2015**, *44*,

7968–7996.

[7] Broadhead, J. A new lithium-non-lithium non-aqueous secondary battery. In *Eighth International Power Sources Symposium, Internat. Power Sources Symposium Committee*, Croydon, Surrey, UK, 1972; pp 287–298.

[8] Wang, Y. L.; Sun, Q. L.; Zhao, Q. Q.; Cao, J. S.; Ye, S. H. Rechargeable lithium/iodine battery with superior high-rate capability by using iodine-carbon composite as cathode. *Energy Environ. Sci*. **2011**, *4*, 3947–3950.

[9] Zhao, Q.; Lu, Y. Y.; Zhu, Z. Q.; Tao, Z. L.; Chen, J. Rechargeable lithium-iodine batteries with iodine/nanoporous carbon cathode. *Nano Lett*. **2015**, *15*, 5982–5987.

[10] Gong, D. C.; Wang, B.; Zhu, J. Y.; Podila, R.; Rao, A. M.; Yu, X. Z.; Xu, Z.; Lu, B. N. An iodine quantum dots based rechargeable sodium-iodine battery. *Adv. Energy Mater*. **2017**, *7*, 1601885.

[11] Tian, H. J.; Gao, T.; Li, X. G.; Wang, X. W.; Luo, C.; Fan, X. L.; Yang, C. Y.; Suo, L. M.; Ma, Z. H.; Han, W. Q. et al. High power rechargeable magnesium/iodine battery chemistry. *Nat. Commun*. **2017**, *8*, 14083.

[12] Tian, H. J.; Zhang, S. L.; Meng, Z.; He, W.; Han, W.-Q. Rechargeable aluminum/iodine battery redox chemistry in ionic liquid electrolyte. *ACS Energy Lett*. **2017**, *2*, 1170–1176.

[13] Zhao, Y.; Wang, L. N.; Byon, H. R. High-performance rechargeable lithium-iodine batteries using triiodide/iodide redox couples in an aqueous cathode. *Nat. Commun*. **2013**, *4*, 1896.

[14] Zhao, Y.; Byon, H. R. High-performance lithium-iodine flow battery. *Adv. Energy Mater*. **2013**, *3*, 1630–1635.

[15] Yamamoto, T.; Hishinuma, M.; Yamamoto, A. Zn | ZnI_2 | iodine secondary battery using iodine-nylon-6 adduct as positive electrode, and its charge-discharge performance. *Inorg. Chim. Acta* **1984**, *86*, L47–L49.

[16] Li, B.; Nie, Z. M.; Vijayakumar, M.; Li, G. S.; Liu, J.; Sprenkle, V.; Wang, W. Ambipolar zinc-polyiodide electrolyte for a high-energy density aqueous redox flow battery. *Nat. Commun*. **2015**, *6*, 6303.

[17] Lee, J.; Srimuk, P.; Fleischmann, S.; Ridder, A.; Zeiger, M.; Presser, V. Nanoconfinement of redox reactions enables rapid zinc iodide energy storage with high efficiency. *J. Mater. Chem. A* **2017**, *5*, 12520–12527.

[18] Puri, B. R.; Bansal, R. C. Iodine adsorption method for measuring surface area of carbon blacks. *Carbon* **1965**, *3*, 227–230.

[19] Moser, J. R. Solid state lithium-iodine primary battery. U.S. Patent 3,660,163, May 2, 1972.

[20] See, K. A.; Gerbec, J. A.; Jun, Y.-S.; Wudl, F.; Stucky, G. D.; Seshadri, R. A high capacity calcium primary cell based on the Ca–S system. *Adv. Energy Mater*. **2013**, *3*, 1056–1061.

[21] Kiefer, W.; Bernstein, H. J. The UV-laser excited resonance Raman spectrum of the I_3^- ion. *Chem. Phys. Lett*. **1972**, *16*, 5–9.

[22] Pang, Q.; Liang, X.; Kwok, C. Y.; Nazar, L. F. Advances in lithium–sulfur batteries based on multifunctional cathodes and electrolytes. *Nat. Energy* **2016**, *1*, 16132.

[23] Aurbach, D.; Pollak, E.; Elazari, R.; Salitra, G.; Kelley, C. S.; Affinito, J. On the surface chemical aspects of very high energy density, rechargeable Li–sulfur batteries. *J. Electrochem. Soc*. **2009**, *156*, A694–A702.

[24] Xu, J. T.; Ma, J. M.; Fan, Q. H.; Guo, S. J.; Dou, S. X. Recent progress in the design of advanced cathode materials and battery models for high-performance lithium-X (X = O_2, S, Se, Te, I_2, Br_2) batteries. *Adv. Mater*. **2017**, *29*, 1606454.

[25] Reddy, T. B. *Linden's Handbook of Batteries*; 4th ed. The McGraw-Hill Companies, Inc.: New York, 2010; pp15.10–15.11.

[26] Dong, X. L.; Chen, L.; Su, X. L.; Wang, Y. G.; Xia, Y. Y. Flexible aqueous lithium-ion battery with high safety and large volumetric energy density. *Angew. Chem., Int. Ed*. **2016**, *55*, 7474–7477.

[27] Suo, L. M.; Borodin, O.; Sun, W.; Fan, X. L.; Yang, C. Y.; Wang, F.; Gao, T.; Ma, Z. H.; Schroeder, M.; von Cresce, A. et al. Advanced high-voltage aqueous lithium-ion battery enabled by "water-in-Bisalt" electrolyte. *Angew. Chem., Int. Ed*. **2016**, *55*, 7136–7141.

[28] Wang, F.; Suo, L. M.; Liang, Y. J.; Yang, C. Y.; Han, F. D.; Gao, T.; Sun, W.; Wang, C. S. Spinel $LiNi_{0.5}Mn_{1.5}O_4$ cathode for high-energy aqueous lithium-ion batteries. *Adv. Energy Mater*. **2017**, *7*, 1600922.